09

m-line method for reflectometry of ultrathin layers

© A.B. Sotsky,[1] E.A. Chudakov,[1] A.B. Shilov,[1] L.I. Sotskaya[2]

[1] Kuleshov State University,
212022 Mogilev, Belarus
[2] Belarusian-Russian University 212000 Mogilev, Belarus
e-mail: ab_sotsky@mail.ru

Received July 19, 2023
Revised October 5, 2023
Accepted October 23, 2023

A solution to the vector electrodynamic problem of describing the intensity distribution of a coherent light beam reflected from a plane-layered medium is obtained. The conditions for observing *m*-lines in the named distribution upon reflection of a Gaussian beam from an ultrathin (nanoscale) layer on the substrate are determined. It has been established that the contrast of *m*-lines is very sensitive to the thickness of such a layer. On this basis, a new method for controlling the thickness and refraction index of ultrathin layers has been proposed. Its features include local layer control, the absence of a reference signal and the absence of the need for mechanical rotation of the sample, contributing to the stability of measurements. An analysis of method errors was performed. Experiments on observing and processing *m*-lines when solving the inverse optical problem for oxide layers on a silicon surface are presented. The results are compared with multi-angle coherent ellipsometry data

Keywords: reflectometry, ultrathin layer, *m*-line, inverse optical problem, Zenneck mode, focused light beam, oxide layer on silicon.

DOI: 10.21883/0000000000

Introduction

Optical methods for monitoring the characteristics of ultrathin layers are in demand in microelectronics and optics. Among them, the most common methods are spectrophotometry [1,2] and spectral ellipsometry [3]. However, in their classical version, these methods involve the use of light beams with a diameter of the millimeter order, which makes local probing of layers difficult. In addition, their application is complicated by the need to find a dispersion of structure materials. The last limitation is absent in the coherent multi-angle methods of ellipsometry [4] and reflectometry [5,6]. But usually these methods involve the use of wide monochromatic beams and mechanical rotation of the sample, which negatively affects the measurement speed and introduces noise into the detected signal. The most interesting method of reflectometry is the version where local probing of layers is carried out through the use of a laser beam focused by a short-focus lens [7]. With normal incidence of such a beam on the layer, it is possible to process intensity distributions for *s*- and *p*-polarization waves reflected from the layer in a wide range of spatial frequencies. But to effectively solve the inverse optical problem of determining the parameters of a layer, the distribution data must contain interference fringes, which imposes a limitation on the minimum layer thickness [7]. The approach can be generalized to the case of using partially coherent radiation [8,9], does not require mechanical rotation of the sample, and is rapid-test-one. However, its practical implementation requires a complex optical design [7–9]. In addition, the rationale for his work is based on a crude plane-wave model [8,9]. A simpler instrumental implementation is the method of local reflectometry of ultrathin layers, which uses a focused laser beam incident on the layer at angles close to the Brewster angle. In [10] considered and a qualitatively justified version of this method with registration of the angular dependence of the integral reflection coefficient on the p-polarized Gaussian beam layer. Its disadvantage is the need for mechanical rotation of the sample.

In this work, we consider the method of layer reflectometry with a focused beam, free from this limitation. Its prototype is a method of waveguide spectroscopy of layers, based on the analysis of the intensity distribution of a laser beam reflected from a prism communication device at a fixed angle of incidence [11]. The analysis is carried out within the *m*-line in the form of two maxima and a central minimum of the named distribution, observed during resonant excitation of the waveguide mode of the layer [11,12]. However, the classical method of waveguide spectroscopy is a contact one, which leads to a distorting effect on the measurement results of the coupling prism. In addition, effective excitation of waveguide modes requires an extended (millimeter-scale) region of optical contact of the coupling prism with the structure under study, which excludes the possibility of local diagnostics of layers. It is shown below that these limitations can be overcome by using a non-contact version of waveguide spectroscopy, which does not require the use of a coupling prism. In it, local probing of the layer is carried out due to the excitation

of Zenneck modes TM or TE polarization in the structure by a laser beam focused directly on the surface of the layer. The beam axis makes an angle with the normal to this surface, close to the angle of zero reflection of a plane wave. Under certain conditions, the intensity distribution of the beam reflected from the layer has, as in standard waveguide spectroscopy, the form of an *m*-line. The *m*-line contour, measured by the photodetector array, is extremely sensitive to the characteristics of the layer. The contour is processed using the least squares method without using a reference signal and without mechanical rotation of the sample. The objective function is constructed based on the solution of the vector electrodynamic problem of the reflection of a limited coherent light beam from a plane-layered medium. Estimates of the errors in solving the inverse optical problem of determining the parameters of oxide layers on the silicon surface are obtained. An experimental verification of the proposed method was carried out for oxide layers of various thicknesses.

1. Mathematical model of non-contact waveguide spectroscopy of the layer

The optical scheme of non-contact waveguide spectroscopy of the layer is shown in Fig. 1, *a*. An incident linearly polarized laser beam is focused by a short-focus lens *O*onto the surface of the layer of thickness d, under study located on the substrate. The structure of the substrate-layer is considered non-magnetic and is described by the relative dielectric permittivity $\varepsilon(y)$. In a homogeneous region, $y > 0$, $\varepsilon = \varepsilon_a$, where ε_a is a real constant. With $j < 0$ the $\varepsilon(y)$ function can be complex. The beam axis makes an angle θ with the normal to the layer. The intensity distribution of the reflected beam $S(x, y')$ is recorded by a matrix of photodetectors Φ, orthogonal to the beam axis and located at a distance D along the beam axis from the layer surface.

Calculation of the $S(x, y')$ function , which has the meaning of a component of the Poynting vector, the normal plane of the matrix Φ, will be performed using a method that is a modification of the approach used in [12] in justifying the technique of standard waveguide spectroscopy.

When considering the reflection of a coherent light beam with a time factor $\exp(i\omega t)$ (this factor is omitted from now on) from the layered medium in the diagram of Fig. 1, *a* we will look for the electromagnetic field in the form of Fourier integrals over spatial frequencies k_x and k_y:

$$\begin{Bmatrix}\mathbf{E}(x,y,z)\\ \mathbf{H}(x,y,z)\end{Bmatrix} = \int_{-\infty}^{\infty} dk_x \int_{-\infty}^{\infty} dk_z \exp(-ik_x x - ik_z z) \times \begin{Bmatrix}\hat{\mathbf{E}}(k_x,k_z,y)\\ \hat{\mathbf{H}}(k_x,k_z,y)\end{Bmatrix}.$$

This field can be represented by a superposition of waves *s*- and *p*-polarization:

$$\mathbf{E} = \mathbf{E}^{(s)} + \mathbf{E}^{(p)}, \qquad \hat{\mathbf{E}} = \hat{\mathbf{E}}^{(s)} + \hat{\mathbf{E}}^{(p)},$$
$$\mathbf{H} = \mathbf{H}^{(s)} + \mathbf{H}^{(p)}, \qquad \hat{\mathbf{H}} = \hat{\mathbf{H}}^{(s)} + \hat{\mathbf{H}}^{(p)}, \tag{1}$$

For waves of *s*-polarization

$$\hat{E}_y^{(s)} \equiv 0, \qquad \hat{E}_z^{(s)} = -\frac{k_x}{k_z}\hat{E}_x^{(s)}, \tag{2}$$

$$\hat{H}_x^{(s)} = \frac{k_x}{k_z}\hat{H}_z^{(s)}, \qquad \hat{H}_y^{(s)} = \frac{1}{\omega\mu_0}\frac{k_x^2 + k_z^2}{k_z}\hat{E}_x^{(s)},$$
$$\hat{H}_z^{(s)} = \frac{1}{i\omega\mu_0}\frac{d\hat{E}_x^{(s)}}{dy}, \tag{3}$$

$$\frac{d^2}{dy^2}\hat{E}_x^{(s)} + \left[k_0^2\varepsilon(y) - k_x^2 - k_y^2\right]\hat{E}_x^{(s)} = 0, \tag{4}$$

where $k_0 = 2\pi/\lambda$ and μ_0 — wave number and magnetic permeability of vacuum

In a homogeneous region $y > 0$, where $\varepsilon = \varepsilon_a$, the solution to equation (4) has the form

$$\hat{E}_x^{(s)} = e_i \exp\left(ik_y^{(a)} y\right) + e_r \exp\left(-ik_y^{(a)} y\right), \tag{5}$$

where

$$e_{i,r} = \frac{1}{(2\pi)^2}\int_{-\infty}^{\infty} dk_x \int_{-\infty}^{\infty} dk_z \exp(ik_x x + ik_z z) E_{i,rx}^{(s)}(x, 0, z),$$

$k_y^{(a)} = \sqrt{k_0^2\varepsilon_a - k_x^2 - k_z^2}$, $E_{ix}^{(s)}(x, 0, z)$ and $E_{rx}^{(s)}(x, 0, z)$ — distributions of the components of the incident and reflected field *s*-polarization on the surface of the $y = 0$ layer. In a homogeneous region $y < -d$, where $\varepsilon = \varepsilon_s$, in accordance with the Sommerfeld radiation condition

$$\hat{E}_x^{(s)} = e_t \exp(ik_y^{(s)} y), \tag{6}$$

where $k_y^{(s)} = \sqrt{k_0^2\varepsilon_s - k_x^2 - k_z^2}$, $\mathrm{Re}k_y^{(s)} \geq 0$,

$$e_t = \frac{1}{(2\pi)^2}\int_{-\infty}^{\infty} dk_x \int_{-\infty}^{\infty} dk_z \exp(ik_x x + ik_z z) E_x^{(s)}(x, -d, z),$$

$E_x^{(s)}(x, -d, z)$ — distribution of the component of the field transmitted through the layer at its lower boundary. Within the $-d \leq y \leq 0$ layer

$$\begin{pmatrix}\hat{E}_x^{(s)}(y)\\ \hat{E}_x^{(s)'}(y)\end{pmatrix} = \begin{pmatrix}L_{11}^{(s)}(y) & L_{12}^{(s)}(y)\\ L_{21}^{(s)}(y) & L_{22}^{(s)}(y)\end{pmatrix}\begin{pmatrix}e_t\\ ik_y^{(s)} e_t\end{pmatrix}, \tag{7}$$

where $\hat{E}_x^{(s)^t} = d\hat{E}_x^{(s)}/dy$, $\mathbf{L}^{(s)}(y)$ — matrix of the fundamental solution of equation (4) [13].

Due to (5)–(7) and the continuity condition of the functions $\hat{E}_x^{(s)}(y)$ and $\hat{E}_x^{(s)^t}(y)$ that follows from (4), the

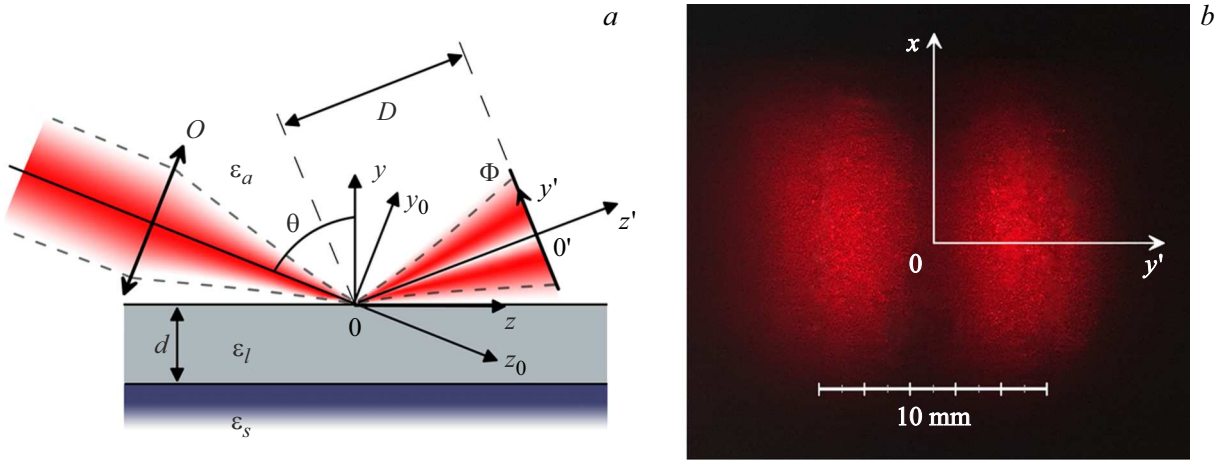

Figure 1. *a* — optical scheme of non-contact waveguide spectroscopy and coordinate systems used in the calculations: intrinsic coordinate system of the incident beam $0xy_0z_0$, coordinate system of the structure layer – substrate and coordinate system $0'xy'z'$ of the photodetector matrix Φ; *b* — photograph of the intensity distribution of the reflected laser beam with the *m*-line structure in the plane of the photodetector matrix Φ.

reflection coefficients from the layer of plane waves that make up the incident beam are equal

$$r_s(k_x, k_z) = \frac{e_r}{e_i} = \frac{ik_y^{(a)}[L_{11}^{(s)}(0) + ik_y^{(s)}L_{12}^{(s)}(0)] - L_{21}^{(s)}(0) - ik_y^{(s)}L_{22}^{(s)}(0)}{ik_y^{(a)}[L_{11}^{(s)}(0) + ik_y^{(s)}L_{12}^{(s)}(0)] + L_{21}^{(s)}(0) + ik_y^{(s)}L_{22}^{(s)}(0)}. \quad (8)$$

In the case of an arbitrary dependence $\varepsilon(y)$, the matrix $\mathbf{L}^{(s)}(y)$ can be calculated numerically using the Runge–Kutta method [14]. For the homogeneous layer model, when $\varepsilon = \varepsilon_l = \text{const}$, at $-d \le y \le 0$in (11) we have [14]:

$$L_{11}^{(s)}(0) = L_{22}^{(s)}(0) = \cos(\sigma d), \quad L_{12}^{(s)}(0) = \sin(\sigma d)/\sigma,$$

$$L_{21}^{(s)}(0) = -\sigma \sin(\sigma d), \quad (9)$$

where $\sigma = \sqrt{k_0^2\varepsilon_l - k_x^2 - k_z^2}$.

For waves *p*-polarization $\mathbf{E} = \mathbf{E}^{(p)}$, $\hat{\mathbf{E}} = \hat{\mathbf{E}}^{(p)}$, $\mathbf{H} = \mathbf{H}^{(p)}$, $\hat{\mathbf{H}} = \hat{\mathbf{H}}^{(p)}$,

$$H_y^{(p)} \equiv 0, \qquad \hat{H}_z^{(p)} = -\frac{k_x}{k_z}\hat{H}_x^{(p)}, \quad (10)$$

$$\hat{E}_x^{(p)} = \frac{k_x}{k_z}\hat{E}_z^{(p)}, \quad \hat{E}_y^{(p)} = -\frac{k_x^2 + k_z^2}{i\omega\varepsilon\varepsilon_0 k_z}\hat{H}_x^{(p)},$$

$$\hat{E}_z^{(p)} = -\frac{1}{i\omega\varepsilon\varepsilon_0}\frac{d}{dy}\hat{H}_x^{(p)}, \quad (11)$$

$$\varepsilon\frac{d}{dy}\frac{1}{\varepsilon}\frac{d}{dy}\hat{H}_x^{(p)} + \left[k^2(y) - k_x^2 - k_y^2\right]\hat{H}_x^{(p)} = 0, \quad (12)$$

where ε_0 — dielectric permittivity of vacuum. For $y > 0$

$$\hat{H}_x^{(p)} = h_i \exp\left(ik_y^{(a)}y\right) + h_r \exp\left(-ik_y^{(a)}y\right), \quad (13)$$

$$h_{i,r} = \frac{1}{(2\pi)^2}\int_{-\infty}^{\infty} dk_x \int_{-\infty}^{\infty} dk_z \exp(ik_x x + ik_z z) H_{i,rx}^{(p)}(x, 0, z), \quad (14)$$

$H_{ix}^{(p)}(x, 0, z)$ and $H_{rx}^{(p)}(x, 0, z)$ — distributions of the components of the incident and reflected field *p*-polarization on the surface of the $y = 0$. Analogues of expressions (6)–(9) are

$$\hat{H}_x^{(p)} = h_t \exp(ik_y^{(s)}y),$$

$$h_t = \frac{1}{(2\pi)^2}\int_{-\infty}^{\infty} dk_x \int_{-\infty}^{\infty} dk_z \exp(ik_x x + ik_z z) H_x^{(p)}(x, -d, z),$$

$$\begin{pmatrix} \hat{H}_x^{(p)}(y) \\ \hat{H}_x^{(p)'}(y) \end{pmatrix} = \begin{pmatrix} L_{11}^{(p)}(y) & L_{12}^{(p)}(y) \\ L_{21}^{(p)}(y) & L_{22}^{(p)}(y) \end{pmatrix} \begin{pmatrix} h_t \\ h_t ik_y^{(s)}/\varepsilon_s \end{pmatrix},$$

$$r_p(k_x, k_z) = \frac{h_r}{h_i} - \left\{(ik_y^{(a)}/\varepsilon_a)\left[L_{11}^{(p)}(0) + (ik_y^{(s)}/\varepsilon_s)L_{12}^{(p)}(0)\right] - L_{21}^{(p)}(0) - (ik_y^{(s)}/\varepsilon_s)L_{22}^{(p)}(0)\right\} / \left\{(ik_y^{(a)}/\varepsilon_a)\left[L_{11}^{(p)}(0) + (ik_y^{(s)}/\varepsilon_s)L_{12}^{(p)}(0)\right] + L_{21}^{(p)}(0) + (ik_y^{(s)}/\varepsilon_s)L_{22}^{(p)}(0)\right\}. \quad (15)$$

$$L_{11}^{(s)}(0) = L_{22}^{(s)}(0) = \cos(\sigma d), \quad L_{12}^{(s)}(0) = \varepsilon_l \sin(\sigma d)/\sigma,$$

$$L_{21}^{(s)}(0) = -\sigma \sin(\sigma d)/\varepsilon_l, \quad (16)$$

The required function $S(x, y')$ has the form

$$S(x, y') = 0.5\text{Re}\left[(E_{rz}H_{rx}^* - E_{rx}H_{rz}^*)\cos\theta + (E_{rx}H_{ry}^* - E_{ry}H_{rx}^*)\sin\theta\right], \quad (17)$$

where the asterisk means complex conjugation, and the vectors of the field reflected from the structure appear

$$\begin{Bmatrix}\mathbf{E}_r\\ \mathbf{H}_r\end{Bmatrix} = \int\limits_{-\infty}^{\infty} dk_x \int\limits_{-\infty}^{\infty} dk_z \exp(-ik_x x - ik_z z - ik_y^{(a)} y) \begin{Bmatrix}\hat{\mathbf{E}}_r\\ \hat{\mathbf{H}}_r\end{Bmatrix}, \tag{18}$$

calculated at

$$y = D\cos\theta + y'\sin\theta, \qquad z = D\sin\theta - y'\cos\theta. \tag{19}$$

According to(1)–(3), (8), (10), (11), (15):

$$\hat{E}_{rx} = h_i \frac{r_p k_x k_y^{(a)}}{k_z \omega \varepsilon_0 \varepsilon_a} + e_i r_s, \quad \hat{E}_{ry} = -h_i \frac{r_p (k_x^2 + k_z^2)}{k_z \omega \varepsilon_0 \varepsilon_a},$$

$$\hat{E}_{rz} = h_i \frac{r_p k_y^{(a)}}{\omega \varepsilon_0 \varepsilon_a} - e_i \frac{r_s k_x}{k_z}, \tag{20}$$

$$\hat{H}_{rx} = h_i r_p - e_i \frac{r_s k_x k_y^{(a)}}{k_z \omega \mu_0}, \quad \hat{H}_{ry} = e_i \frac{r_s (k_x^2 + k_z^2)}{k_z \omega \mu_0},$$

$$\hat{H}_{rz} = -e_i \frac{r_s k_y^{(a)}}{\omega \mu_0} - h_i \frac{r_p k_x}{k_z}. \tag{21}$$

The functions $e_i(k_x, k_z)$, $h_i(k_x, k_z)$ included in (20), (21) can be expressed in terms of the electric field components of the incident beam $E_{xi}(x, 0, z)$, $E_{y0i}(x, 0, z)$ in its own coordinate system $0xy_0z_0$ (Fig. 1, *a*):

$$e_i = \hat{E}_{xi} \frac{k_z \left[(k_x^2 + k_z^2)\sin\theta + k_z k_y^{(a)} \cos\theta\right]}{(k_x^2 + k_z^2)(k_z \sin\theta + k_y^{(a)} \cos\theta)}$$

$$- \hat{E}_{y_0 i} \frac{k_x k_y^{(a)} k_z}{(k_x^2 + k_z^2)(k_z \sin\theta + k_y^{(a)} \cos\theta)}, \tag{22}$$

$$h_i = -\hat{E}_{xi} \frac{\omega \varepsilon_0 \varepsilon_a k_x k_z \cos\theta}{(k_x^2 + k_z^2)(k_z \sin\theta + k_y^{(a)} \cos\theta)}$$

$$- \hat{E}_{y_0 i} \frac{\omega \varepsilon_0 \varepsilon_a k_z^2}{(k_x^2 + k_z^2)(k_z \sin\theta + k_y^{(a)} \cos\theta)}, \tag{23}$$

where

$$\begin{Bmatrix}\hat{E}_{xi}\\ \hat{E}_{y_0 i}\end{Bmatrix} = \frac{1}{(2\pi)^2} \int\limits_{-\infty}^{\infty} dx \int\limits_{-\infty}^{\infty} dz$$

$$\times \exp(ik_x x + ik_z z) \begin{Bmatrix}E_{xi}(x, 0, z)\\ E_{y_0 i}(x, 0, z)\end{Bmatrix}. \tag{24}$$

Let the structure be excited by a Gaussian beam, the amplitude radius of which in the waist located in the $z_0 = 0$ plane is equal to w. The electric field of the beam in a given plane is linearly polarized. The direction of its oscillations makes an angle α with the plane of incidence $x = 0$. Let's use the model [15]:

$$\begin{Bmatrix}E_{xi}(x, 0, z)\\ E_{y_0 i}(x, 0, z)\end{Bmatrix} = A \exp\left[-\left(\frac{x}{w}\right)^2 - \left(\frac{z\cos\theta}{w}\right)^2 - ik_0 n_a z \sin\theta\right] \begin{Bmatrix}\sin\alpha\\ \cos\alpha\end{Bmatrix}, \tag{25}$$

where A — beam amplitude, $n_a = \sqrt{\varepsilon_a}$. Then, in accordance with (24), (25):

$$\begin{Bmatrix}\hat{E}_{xi}\\ \hat{E}_{y_0 i}\end{Bmatrix} = \frac{Aw^2}{4\pi \cos\theta} \exp\left\{-\left(\frac{k_x w}{2}\right)^2 - \left[\frac{(k_z - k_0 n_a \sin\theta)w}{2\cos\theta}\right]^2\right\} \begin{Bmatrix}\sin\alpha\\ \cos\alpha\end{Bmatrix}. \tag{26}$$

According to (17)–(23), (26), finding the function $S(x, y')$ is reduced to calculating six integrals of the same type

$$I(x, y') = \int\limits_{-\infty}^{\infty} d\varsigma \int\limits_{-\infty}^{\infty} d\xi \exp\left\{-\left(\frac{\xi k_0 w}{2}\right)^2 - \left[\frac{(\varsigma - n_a \sin\theta)k_0 w}{2\cos\theta}\right]^2 - ik_0(\xi x + \varsigma z + \eta y)\right\} F(\xi, \varsigma), \tag{27}$$

where $\xi = k_x/k_0$, $\varsigma = k_z/k_0$, $\eta = \sqrt{\varepsilon_a - \xi^2 - \varsigma^2}$, $\mathrm{Re}\eta > 0$. The explicit form of the function $F(\xi, \varsigma)$ for each of the components of the field $\mathbf{E_r}$, $\mathbf{H}_r$ is obvious from (20)–(23), (26).

From the standpoint of waveguide spectroscopy of the layer, the main interest is to study the $S(x, y')$ function at $x = 0$, when it may have the structure of the *m*-line [11]. But due to the natural conditions of $k_0 D \gg 1$, and therefore $k_0 y \gg 1$, $k_0 z \gg 1$ (see (19)), direct numerical calculation of $I(0, y')$and$S(0, y')$ is complicated by rapid fluctuations of the exponential function in (27). This problem can be partially overcome by deforming the integration contour in the inner integral in (27) to the contour of the fastest descent. In standard waveguide spectroscopy, the formation of the *m*-line is explained by the proximity of the saddle point of the fastest descent contour to the poles of the functions$r_s(k_x, k_z)$, $r_p(k_x, k_z)$ located at the zeros of the dispersion equations for the modes of the structure flowing into the coupling prism [12]. In non-contact waveguide spectroscopy, the coupling prism and such poles are absent. As a result, no complications arise with the indicated deformation, and expression (27) is reduced to the form

$$I(0, y') = \int\limits_{-\infty}^{\infty} d\varsigma \exp[f(\varsigma)] \int\limits_{-\infty}^{\infty} d\tau \exp(-\tau^2) \frac{d\xi}{d\tau} F(\xi, \varsigma), \tag{28}$$

where

$$f(\varsigma) = -\left[\frac{(\varsigma - n_a \sin\theta)k_0 w}{2\cos\theta}\right]^2 - ik_0\varsigma z - ik_0 ky, \quad (29)$$

$$\xi = \frac{2\tau}{k_0}\sqrt{\frac{2ikk_0 y + \tau^2}{2y^2 + w^2 q + \sqrt{(2y^2 + w^2 q)^2 - w^4(q^2 + k^2 k_0^2 y^2)}}},$$

$$\frac{d\xi}{d\tau} = \frac{4\tau(4q - \xi^2 k_0^2 w^2)}{\xi[8k_0^2 y^2 + k^2 w^2(4q - \xi^2 k_0^2 w^2)]},$$

$$q = ikk_0 y + \tau^2, \qquad k = \sqrt{\varepsilon_a - \varsigma^2}.$$

Formula (28) is strict and allows you to perform a numerical calculation of the $I(0, y')$ values in a time of about a minute. But in the outer integral in (28), fast oscillations of the exponential function are not completely eliminated, which makes representation (28) of little use in solving the inverse optical problem of determining the layer parameters, which is much more extensive than a single calculation of the function$I(0, y')$.

To further simplify the calculations, we apply the saddle point method [16] consistently to the inner and outer integrals in (28)). As a result, we arrive at the analytical approximation

$$I(0, y') = -\frac{4\pi k^2 \cos\theta \exp[f(\varsigma_s)]F(0, \varsigma_s)}{\sqrt{(2ik_0 y - k_0^2 w^2 k)(2ik_0 y\varepsilon_a \cos^2\theta - k_0^2 w^2 k^3)}} \times [1 + O(k_0 D)^{-1}], \quad (30)$$

where $k = \sqrt{\varepsilon_a - \varsigma_s^2}$, ς_s — root of the equation

$$ik_0(\varsigma_s y - kz)2\cos^2\theta - k(\varsigma_s - n_a \sin\theta)k_0^2 w^2 = 0. \quad (31)$$

In the calculations presented below, the numerical solution of equation (31) was obtained by the contour integration method [12].

In approximation (30), the function $S(0, y')$ has the form suitable for solving the inverse optical problem:

$$S(0, y') = |A|^2 w^4 k_0^5 (2\omega\mu_0)^{-1} \bar{S}(y'), \quad (32)$$

$$\bar{S}(y') = \frac{k^4 \exp\{2\mathrm{Re}[f(\xi_s)]\}\,\mathrm{Re}(G\sin^2\alpha|r_s|^2 + \varepsilon_a G^{-1}\cos^2\alpha|r_p|^2)}{|(2ik_0 y - k_0^2 w^2 k)(2ik_0 y\varepsilon_a \cos^2\theta - k_0^2 w^2 k^3)|}, \quad (33)$$

where $G = \xi_s \sin\theta + k\cos\theta$; r_s and r_p are calculated at $k_x = 0$, $k_z = k_0\xi_s$. According to (32), (33), at $\alpha = 0$ the $S(0, y')$ function is formed by p- waves, and at $\alpha = \pi/2$by s-polarization waves

The structure of the m-line in the intensity distribution of a Gaussian beam in the plane of the photodetector array after its reflection from an ultrathin layer can be judged from Fig. 2. Here,

$$S_n(y') = S(0, y')/\max[S(0, y')].$$

Table 1. C-observation criterion m-lines for differentSiO_2 layer thicknesses and beam radii

d, nm	w, μm	R	$\partial^2 R/\partial\theta^2$	C
4	2	0.0013	7.38	0.07
4	5	0.0013	7.38	0.44
4	8	0.0013	7.38	1.12
0	5	$5.8 \cdot 10^{-6}$	7.45	0.002
1	5	$1.2 \cdot 10^{-4}$	7.44	0.039
7	5	0.0038	7.27	1.27
8	5	0.0048	7.23	1.65
8.2	2.09	0.0051	7.22	0.30
950	2.09	0.022	33.75	0.28

Calculations were performed for a homogeneous SiO_2 layer on a silicon substrate. The values used were $\alpha = 0$, $\lambda = 0.6328\,\mu$m, $n_a = 1.0003$, $D = 5$ cm,, reference data $\varepsilon_l = 1.457^2$, $\varepsilon_s = (3.878 - i0.02)^2$ [17] and the pseudo-Brewster angle of incidence for waves p-polarization

$$\theta = \theta_B = \mathrm{arctg}\sqrt{\mathrm{Re}(\varepsilon_s/\varepsilon_a)} = 75.54^\circ. \quad (34)$$

Figs 2, a compares the functions $S_n(y')$, calculated in approximation (solid curves) and using exact formulas (17), (28) (discrete symbols) for different beam radii. Solid curves and symbols visually coincide, which indicates acceptable accuracy of the approximation (32). On this basis, it was used in all further calculations. It also follows from Fig. 2, a that the form of the m-line for a particular structure depends significantly on the beam radius w , and as w increases, the contrast of the m-line decreases until it completely disappears.

Figs 2, b shows the contours of the m-line corresponding to different thicknesses of theSiO_2 layer at a fixed radius of the probing beam. Here one can note the extremely high sensitivity of the m-line contrast to the layer thickness at nm. However, at nm both the m-line itself and the significant sensitivity of the normalized intensity distribution of the reflected beam to the layer thickness disappear. Thus, non-contact waveguide spectroscopy of ultrathin layers is effective provided that the m-line is observed in the intensity distribution of the reflected beam.

A numerical study of a number of structures has shown that to implement the m-line, a linearly polarized incident beam should be used, and its angle of incidence θ — should be selected from the condition of achieving a minimum plane-wave reflectivity of the layer-substrate structure $R(\theta)$, where

$$R(\theta) = |r_p(0, k_0 n_a \sin\theta)|^2 \quad \text{for} \quad \alpha = 0,$$

$$R(\theta) = |r_s(0, k_0 n_a \sin\theta)|^2 \quad \text{for} \quad \alpha = \pi/2.$$

To evaluate the remaining conditions for obtaining the m-line, we take into account that it is observed in the paraxial region of the far observation zone at $|y'| \ll D$, $k_0 w^2 \ll D$ (Fig. 2). In this case, the approximate solution

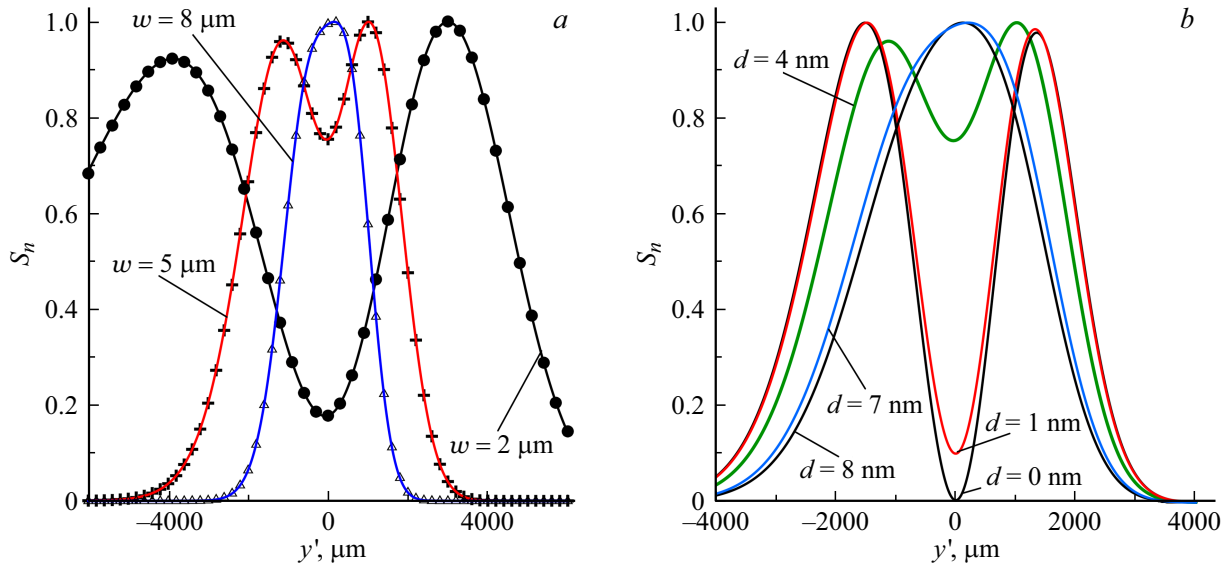

Figure 2. Structure *m*-lines in waveguide spectroscopy of ultrathin layers: *a* — SiO_2 layer of thickness $d = 4$ nm and different beam radii w; *b* — layers SiO_2 of various thicknesses, $w = 5\,\mu$m.

of equation (31) has the form $\xi_s = n_a(\sin\theta - y'\cos\theta/D)$, and in accordance with (29), (32):

$$S_n(y') \sim \exp(-\varepsilon_a k_0^2 w^2 \eta)[R(\theta) + \eta\partial^2 R/\partial\theta^2], \qquad (35)$$

where $\eta = y'^2/(2D^2)$. To obtain (35), the Taylor expansion of the function$R(\theta)$ in the vicinity of its minimum was used, up to two leading terms. Differentiation of function (35) leads to the following conditions for observing the *m*-line: $\partial R/\partial\theta = 0$,

$$C = \frac{\varepsilon_a k_0^2 w^2 R}{\partial^2 R/\partial\theta^2} < 1, \qquad (36)$$

where the function $R(\theta)$ and its derivatives are taken at its minimum point, i.e. $\partial^2 R/\partial\theta^2 > 0$.

The correctness of criterion (36) in relation to the structures considered above is illustrated in Table 1 (lines 2–8). As follows from Table 1, condition (36) is consistent with the shape of all graphs in Fig. 2.

According to (36), *m*-lines can be easily obtained under conditions close to the conditions for excitation of Zenneck modes, i.e. $R \to 0$ [18,19]. For weakly absorbing layers, such conditions can be established analytically according to the scheme considered in [18].

In the case of $\alpha = 0$ (reflection of waves of *p*-polarization) $R(\theta) \to 0$ at $\theta = \theta_B$

$$d = 0.5q\lambda/\sqrt{\mathrm{Re}\varepsilon_l - \varepsilon_a \sin^2\theta_B}, \quad q = 0, 1, \ldots, \qquad (37)$$

where θ is given by the formula (34), and also with

$$\theta = \theta_B = \arcsin\sqrt{0.5a\left(\sqrt{1 - 4b/a^2} - 1\right)/\varepsilon_a}, \qquad (38)$$

$$a = \mathrm{Re}\left[\frac{\varepsilon_l^4(\varepsilon_a + \varepsilon_s) - 2\varepsilon_l\varepsilon_a^2\varepsilon_s^2}{\varepsilon_a^2\varepsilon_s^2 - \varepsilon_l^4}\right],$$

$$b = \mathrm{Re}\left[\frac{\varepsilon_l^2\varepsilon_a\varepsilon_s}{\varepsilon_a\varepsilon_s + \varepsilon_l^2}\right],$$

$$d = 0.25(2q+1)\lambda/\sqrt{\mathrm{Re}\varepsilon_l - \varepsilon_a^2\sin^2\theta_B}, \quad q = 0.1, \ldots, \qquad (39)$$

if:

$$\mathrm{Re}\,(\varepsilon_l - \sqrt{\varepsilon_a\varepsilon_s}) \geq 0. \qquad (40)$$

In the case of $\alpha = \pi/2$ (reflection of *s*-polarization) $R(\theta) \to 0$ under conditions (39),

$$\mathrm{Re}\,(\varepsilon_l - \sqrt{\varepsilon_a\varepsilon_s}) \leq 0, \qquad (41)$$

$$\theta = \theta_B = \arcsin\sqrt{\mathrm{Re}\left[(\varepsilon_l^2/\varepsilon_a - \varepsilon_s)/(2\varepsilon_l - \varepsilon_a - \varepsilon_s)\right]}. \qquad (42)$$

For the above material constants and wavelengths, inequality (40) is violated, and (41) is satisfied. Therefore, according to (34), (37), in the case of reflection from the SiO_2 silicon layer of light beams *p*-polarization *m*-lines will occur at

$$\theta \approx 75.5^\circ,\ d \approx 0,\ 2,\ 9001,\ 581,\ 872,\ 1163\,\text{nm}, \ldots. \qquad (43)$$

Similar values for *s*-polarization beams we find from (39), (42):

$$\theta \approx 70.9^\circ,\ d \approx 143,\ 428,\ 713,\ 999,\ 1284\,\text{nm}, \ldots. \qquad (44)$$

In accordance with (36), observation of *m*-lines is possible even with shallower minima of the$R(\theta)$ dependence than almost zero ones, as when conditions (34), (37) –(39), (42 are met, in the case of using beams of sufficiently small radius (see section 3).

2. Errors in solving the inverse optical problem

Let there be experimental data for the function

$$S_j = S(0, y'_j)/\max_j[S(0, y'_j)],$$

where $y'_j = j\Delta y'$, $j = 0, \pm 1, \ldots, \pm L$. Layer parameters p_k $(k = \overline{2, N})$ will be determined from the condition of the minimum for the objective function

$$F(p_1, p_2, \ldots, p_N) = \sum_{j=-L}^{L} \left[S_j - S_j^{(m)}(p_1, p_2, \ldots, p_N)\right]^2, \tag{45}$$

where $S_j^{(m)} = p_1\bar{S}(y'_j)$ are theoretical values obtained within the framework of the model (32), (33), p_1 — normalization constant, $p_2 = d$, $p_3 = n_l = \mathrm{Re}\sqrt{\varepsilon_l}$, $p_4 = k_l = -\mathrm{Im}\sqrt{\varepsilon_l}$. Parameters p_k satisfy the system of nonlinear equations

$$\sum_{j=-L}^{L} \frac{\partial S_j^{(m)}}{\partial p_i}\left[S_j - S_j^{(m)}(p_1, p_2, \ldots, p_N)\right] = 0 \quad (i = \overline{1, N}). \tag{46}$$

In (45), (46) the values S_j are specified with experimental errors δS_j.. As a result, errors in the δp_kparameters occur. According to (46), in an approximation linear with respect to errors

$$\delta p_k = \sum_{j=-L}^{L} \delta S_j \sum_{i=1}^{N} M_{ki}^{-1} \frac{\partial S_j^{(m)}}{\partial p_i}, \tag{47}$$

where M^{-1} is the matrix inverse to matrix M with elements

$$M_{ik} = \sum_{j=-L}^{L} \frac{\partial S_j^{(m)}}{\partial p_k} \frac{\partial S_j^{(m)}}{\partial p_k}. \tag{48}$$

The coefficients $\partial S_j^{(m)}/\partial p_i$ in (47), (48) are calculated either with exact values values p_k or with p_k, obtained by minimizing the function (45). With $i = \overline{2, N}$ these coefficients are proportional to the derivatives

$$\partial|r_{p,s}|^2/\partial p_i = 2\mathrm{Re}(r^*_{p,s}\partial r_{p,s}/\partial p_i), \tag{49}$$

which are easy to calculate analytically based on (8), (9), (15), (16).

In a real experiment, where when measuring S_j there are rounding errors correlated at different numbers j caused by analog-to-digital conversion, as well as systematic errors associated with the adjustment of the optical circuit, the most correct estimate is the error modules estimate (47) from above:

$$|\delta p_k| \le \max|\delta S_j| E_k, \tag{50}$$

where $\max|\delta S_j|$ — maximum error module δS_j,

$$E_k = \sum_{j=-L}^{L} \left| \sum_{i=1}^{N} M_{ki}^{-1} \frac{\partial S_j^{(m)}}{\partial p_i} \right| \tag{51}$$

— error coefficient for determining the parameter p_k [20].

It is known that inverse optical problems about the simultaneous reconstruction of three parameters d, n_l, k_l $(N = 4)$, or two parameters d, n_l $(N = 3)$ of ultrathin layers are ill-conditioned, therefore, when studying such layers, they are often limited to determining their thickness d $(N = 2)$, considering also given constants [7,8,21 –23]. In this case, it is of interest to estimate the derivatives $\partial d/\partial n_l$, $\partial d/\partial k_l$ which characterize the sensitivity of the reconstructed layer thickness to the errors of the a priori setting n_l and k_l. Similarly (47) we have

$$\partial d/\partial p_k = (M_{21}M_{1k} - M_{11}M_{2k})(M_{11}M_{22} - M_{21}M_{12})^{-1} \quad (k = 3,\ 4). \tag{52}$$

To assess the effectiveness of using m-lines, it is of interest to compare values (51), (52) with similar values that occur in the case of standard coherent reflectometry of layers, where the angular dependences of the reflectivity of the $R(\theta)$ layer are processed for waves of p- or s-polarization. In the latter case, formulas similar to (45)−(48) take place, but instead they contain experimental data for $R(\theta_j)$, and instead of S_j, theoretical data for $|r_p(\theta_j)|^2$, or $|r_s(\theta_j)|^2$ [20]. A similar comparison is presented in Table 2. The above wavelengths and material constants were used in the calculations.

In Table 2, the designation „m-line“ refers to the results obtained by processing m-lines in the intervals of variation y' indicated in Fig. 2, b and Fig. 4 at $\Delta y' \le 20\,\mu$m.. The specific choice of $\Delta y'$ from the specified range did not affect the tabular data, which is explained by the possibility of replacing the sums over j in (48) and (51) with integrals when $\Delta y' \to 0$. For $d = 4$ nm,$w = 5\,\mu$m, $D = 5$ cm, $\theta = 75.54°$; at $d = 8.2$ nm — $w = 2.09\,\mu$m, $D = 5$ cm, $\theta = 75.7°$; at $d = 950$ nm — $w = 2.09\,\mu$m, $D = 7$ cm, $\theta = 61.21°$. The last two sets of constants correspond to the experimental data presented in Section.

The designation „R“ in Table 2 refers to the results of standard coherent reflectometry of layers, which were obtained as a result of scanning the $0° \le \theta \le 90°$ interval with a step of $\Delta\theta \le 0.02°$

As can be seen from Table 2, the$m$-line technique is inferior in accuracy to the results of standard reflectometry (has higher error rates) only when attempting to simultaneously determine three parameters of the ultrathin layer d, n_l, k_l $(N = 4$, cases$d = 4$and 8.2 nm). But when estimating the error in measuring the reflectivity of the layermax $|\delta R\theta_j| \le 0.0005$ [10], in accordance with (50) and Table 2 (mode R, $N = 4$), we have $|\delta p_2| = |\delta d| \le 9$ nm at $d = 4$ nm and $|\delta d| \le 4.9$ nm at $d = 8.2$ nm. Thus, in the$N = 4$ version, both considered reflectometry techniques can lead to unacceptable errors in determining the thickness of nano-sized layers. At the same time, according to Table 2, at $N = 3$ and 2, m-line method is characterized by error coefficients E_2 and E_3 of the order of magnitude 1−3 less than similar coefficients with standard reflectometry.

Table 2. Error coefficients (51) and sensitivity (52) for SiO_2 layers of various thicknesses

d, nm	Polarization	Mode	N	E_2, nm	E_3	E_4	$\partial d/\partial n_l$, nm	$\partial d/\partial k_l$, nm
4	*p*-	*m*-line	4	297 740	74 389	2454	—	—
			3	183	46	—	—	—
			2	10	—	—	−4	0.6
		R	4	18 000	4079	152	—	—
			3	11 000	2424	—	—	—
			2	1600	—	—	−5	−9
8.2	*p*-	*m*-line	4	41 595	5037	327	—	—
			3	180	22	—	—	
			2	19	—	—	−8	3
		R	4	9700	1074	78	—	—
			3	5900	612	—	—	—
			2	840	—	—	−9	−8
950	*s*-	*m*-line	4	327	5	0.21	—	—
			3	29	0.37	—	—	—
			2	17	—	—	64	−7
		R	4	1200	1.2	0.17	—	—
			3	1200	1.2	—	—	—
			2	200	—	—	−960	−90

It also follows from Table 2 that the error in a priori setting the refractive index of the ultrathin layer Δn_l has little effect on the error in determining the layer thickness. Thus, $|\Delta n_l| = 0.1$ induces a modulus of relative deviation of the layer thickness of the order of 10%, both at $d = 4\,\text{nm}$ and at$d = 8.2\,\text{nm}$.

Note also that in real experiments the errors δS_j are unknown. In such a situation, it is possible to minimize $|\delta p_k|$ by choosing experimental conditions that ensure minimum error rates (51) [20].

For example, for a layer SiO_2 of thickness $d = 4\,\text{nm}$, a numerical search for the minimum of the function $E_2(\theta, w, \Delta Y)$ at $N = 2$, $\alpha = 0°$, $D = 5\,\text{cm}$ gives, that $E_{2\,\min} = 9.0\,\text{nm}$ is achieved at optimal $\theta = 75.58°$, $w = 5.01\,\mu\text{m}$, $\Delta Y = 3840\,\mu\text{m}$ (here $\Delta Y = 2L\Delta y'$ — full length experimental range y'). The behavior of the function $E_2(\theta, w, \Delta Y)$ near its minimum can be judged from Fig. 3.

The existence of optimal ones in Fig. 3 is explained by the fact that excessive magnification practically does not provide new information on the layer thickness, but increases the role of experimental errors [20]. The presence of optimal (Fig. 3, *a*) and (Fig. 3, *b*), corresponding to the minimum, is associated with the implementation of the contrast *m*-line.

3. Experiment

In order to test the *m*-line method, experiments were performed for oxide layers of various thicknesses on the silicon surface. Two samples were used, obtained by annealing polished silicon wafers in an oxygen atmosphere for 15 (sample I) and 90 min (sample II), which were studied earlier in [24] by the method of coherent multi-angle ellipsometry at the wavelength $\lambda = 0.6328\,\mu\text{m}$. The radiation source was a single-mode specified He−Ne-circular polarization of the output beam. The polarization of the beam at the input of the lens O (Fig. 1, *a*) was set using a linear polarizer. A PMMA lens with a focal length of 6.5 mm was used. The radius of the focused beam in the $w = 2.05\,\mu$ waist was determined previously from the far-field intensity distribution of the beam. Intensity photometry was carried out using a line of Hamamatsu S13496 photodetectors with a distance between adjacent pixels $7\,\mu\text{m}$. Next, the beam waist at the lens output was aligned with the surface of the layer under study. The sample was rotated until the intensity distribution of the reflected beam in the plane Φ (Fig. 1, *a*) was obtained in a form similar to that shown in Fig. 1, *b*. This distribution was initially observed on a matte surface using a Samsung Galaxy S10 smartphone. Then this surface was replaced by the input plane of the photodetector line array, oriented

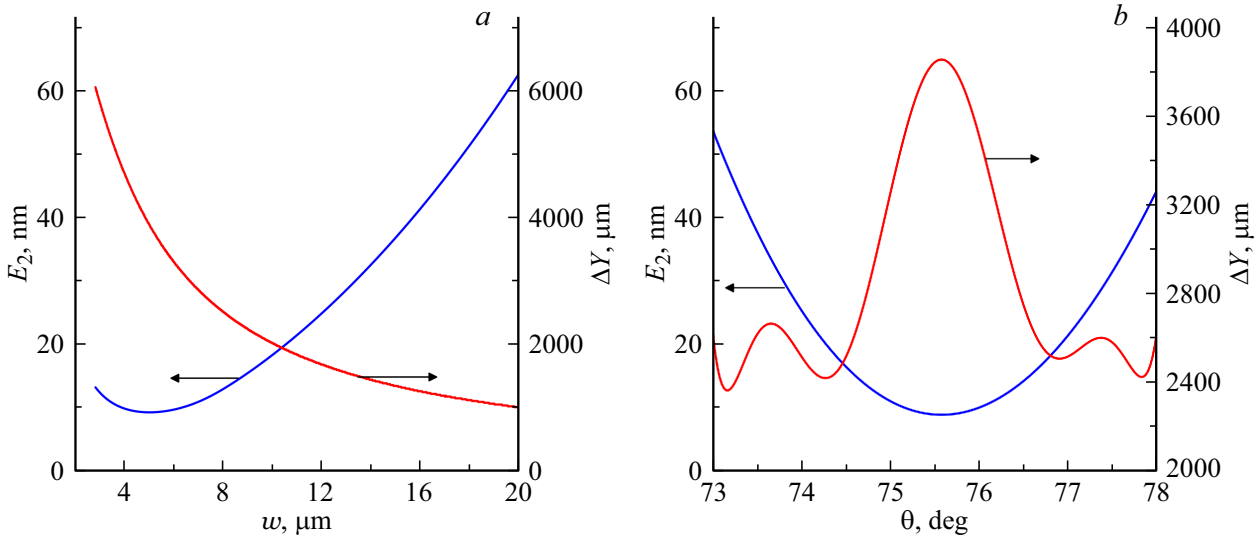

Figure 3. Minimum value and corresponding function argument $E_2(\Delta Y)$, depending w at $\theta = 75.58^\circ$ (a) and depending on θ at $w = 5.01\,\mu$m (b).

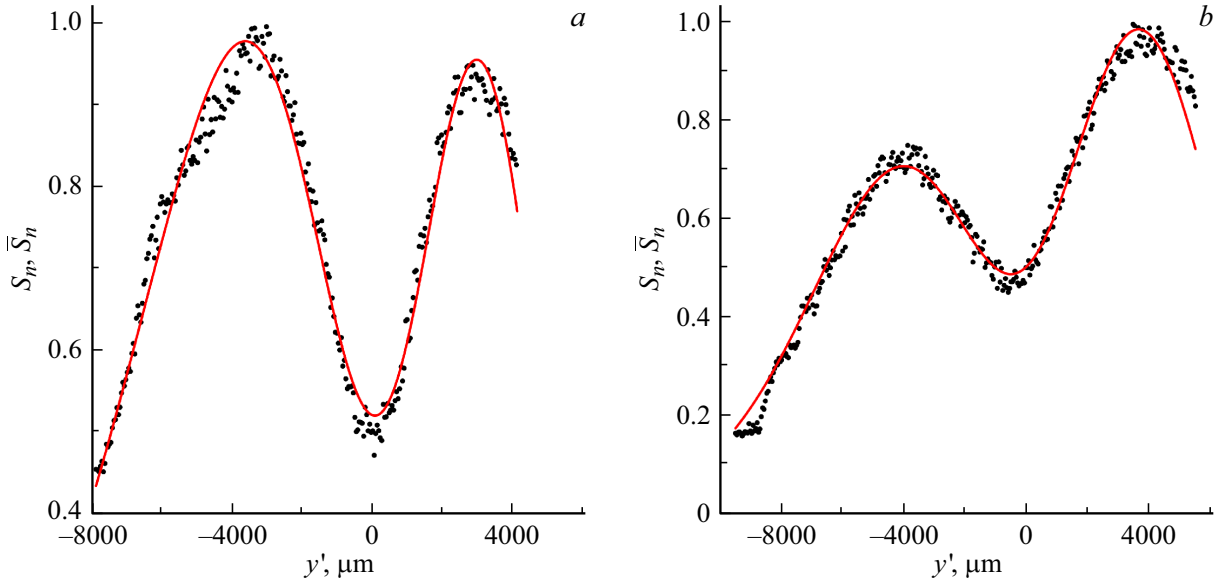

Figure 4. a — theoretical (solid curves) and experimental (discrete points) contours of m-lines for sample I at m, at $\theta = 75.7^\circ$, $D = 5$ cm$b$ — similar data for the sample II at $\theta = 61.21^\circ$, $D = 7$ cm.

along the plane of incidence of the beam, and the intensity distribution $S(0, y'_j)$ was measured. The distance between the sample surface and the array of photodetectors D (Fig. 1, a) was 5 and 7 cm for samples I and II, respectively. The angle of incidence of the beam on the sample was controlled by a goniometer GS-5.

For sample I, the intensity distribution of the reflected beam with the structure m-lines (Fig. 1, b) could be observed only with $\alpha = 0$ p-polarization beam) in the vicinity of the angle of incidence of the$\theta = 75.7^\circ$ beam, close to the Brewster angle. For sample II, similar distributions were obtained only at $\alpha = \pi/2$ (beam of s-polarization) in the vicinity of the angle of incidence IF $\theta = 61.21^\circ$. The theoretical distributions of intensity obtained as a result of finding the minima of the function (45) using the $(\overline{S_n}(y') = p_1\overline{S}(y'))$ gradient method and the experimental intensity distributions with the structure of m-lines are presented in Fig. 4.

The calculations used a model of a homogeneous oxide layer with two variable parameters d and n_l (in (45) $N = 3$). For layer I, as a result of solving the inverse optical problem,$d = 8.2$ nm, $n_l = 1.463$ were obtained, for layer II — $d = 950$ nm, $n_l = 1.458$. These data are in satisfactory agreement with $d = 8.8$ nm, $n_l = 1.453$ for layer I

and ellipsometer's $d = 940$ nm, layer II, layering in [24]. It can be assumed that some discrepancy between the current and previously obtained data is caused by the variability of the thickness of the oxides over the surface of the samples. It is appropriate to note here that in our measurements the area of the probed region on the surface of the $2w^2/\cos\theta$ layer was $34\,\mu\text{m}^2$ for sample I and $17.5\,\mu\text{m}^2$ for sample II.

Note also that, in agreement with the data (43) and (44) for layer I, observation of the *m*-line is possible only when using a beam of *p*-polarization incident at an angle close to the Brewster angle. For layer II, the value closest to its thickness 950 nm is the value $d = 999$ nm from the set (44), which explains the possibility of detecting the *m*-line only when using a beam of *s*-polarization. But the required angle of incidence of such a beam $\theta = 61.21°\text{E}$ differs markedly from that indicated in (44) $\theta = 70.9°$. This is due to the sharp dependence of the angle of minimum reflection of waves of *s*-polarization on the layer thickness. The fulfillment of the criterion for observing *m*-lines (36) for layers I and II is illustrated by the last two rows of Table 1.

Conclusion

A solution to the vector electrodynamic problem of describing the intensity distribution of a coherent light beam reflected from a plane-layered medium is obtained. On its basis, the conditions for observing *m*-lines in the named distribution when the beam is reflected from an ultrathin dielectric layer on the substrate are determined. The structure of these *m*-lines is similar to the structure of the *m*-lines observed in standard waveguide spectroscopy of layers using prism excitation of waveguide modes. However, their observation, being associated with the excitation of Zenneck modes I*p*- or *s*-polarization, does not require a coupling prism. It has been established that the contrast of *m*-lines is very sensitive to the thickness of such a layer. On this basis, a new method for controlling the thickness and refraction index of ultrathin layers has been proposed. Its features include local surface control, the absence of a reference signal, and the absence of the need for mechanical rotation of the sample (besides the alignment of the optical circuit), contributing to the stability of measurements. An analysis of method errors was performed. Their comparison with the error coefficients of the standard method of coherent plane-wave reflectometry confirmed the effectiveness of the developed approach. Experiments on observing and processing *m*-lines when solving the inverse optical problem for oxide layers on a silicon surface are presented. The results of determining the refractive indices and layer thicknesses are in satisfactory agreement with the data of multi-angle coherent ellipsometry.

Funding

The study was executed under the State Program for Scientific Research of the Republic of Belarus „1.15 Photonics and Electronics for Innovations“.

Conflict of interest

The authors declare that they have no conflict of interest.

References

[1] A.V. Tikhonravov, T.V. Amotchkina, M.K. Trubetskov, R.J. Francis, V. Janitski, J. Sancho-Parramon, H. Zorc, V. Pervak. Appl. Opt., **51** (2), 245 (2012). DOI: 10.1364/ao.51.000245
[2] A.B. Sotsky, S.S. Mikheev, N.I. Staskov, L.I. Sotskaya. Opt. i spektr., **128** (8), 1133 (2020) (in Russian). DOI: 10.21883/OS.2020.08.49711.79-20
[3] D.E. Aspnes. Thin Solid Films, **571**, 334 (2014). DOI: 10.1016/j.tsf.2014.03.056
[4] L.A. Fedyukhin, A.V. Gorchakov, E.A. Kolosovsky. Opt. i spektr., **128** (2), 266 (2020) (in Russian). DOI: 10.21883/OS.2020.02.48975.219-19
[5] D.I. Bilenko, A.A. Sagaidachnyi, V.V. Galushka, V.P. Polyanskaya. Tech. Phys., **55** (10), 1478 (2010). DOI: 10.1134/S1063784210100130
[6] I.M. Aliev, S.P. Zinchenko, A.P. Kovtun, G.N. Tolmachev, A.V. Pavlenko. ZhTF, **85** (10), 145 (2015). (in Russian).
[7] A. Rosencwaig, J. Opsal, D.L. Willenborg, S.M. Kelso, J.T. Fanton. Appl. Phys. Lett., **60** (11), 1301 (1992). DOI: 10.1063/1.107323
[8] C. Garam, K. Mingyu, K. Jinyong, J.P. Heui. Opt. Express, **28**, 26908 (2020). DOI: 10.1364/OE.405204
[9] J. Wang, L. Peng, F. Zhai, D. Tang, F. Gao, X. Zhang, R. Chen, L. Zhou, X. Jiang. Opt. Express, **31**, 6552 (2023). DOI: 10.1364/OE.481389
[10] D.C. Holmes, R.P. Johnson. Proc. SPIE, **2337**, 176 (1994). DOI:10.1117/12.186643
[11] A.V. Khomchenko. *Waveguide Spectroscopy of Thin Films* (Academic Press, Amsterdam, 2005)
[12] A.B. Sotsky. *Teoriya opticheskilh volnovodnykh elementov* (UO „MGU im. A.A. Kuleshov“, Mogilev, 2011) (in Russian)
[13] E. Kamke. *Spravochnik po obyknovennym differentsial'nym uravneniyam* (Nauka, M., 1951) (in Russian).
[14] A.B. Sotsky, S.S. Mikheev, N.I. Staskov, L.I. Sotskaya. Opt. i spektr., **128** (8), 1133 (2020) (in Russian). DOI: 10.21883/OS.2020.08.49711.79-20
[15] R. Ulrich. J. Opt. Soc. Am., **20** (10), 1337 (1970). DOI: 10.1364/JOSA.60.001337
[16] V.I. Smirnov. *Kurs vysshey matematiki*, t. 3, ch. 2 (BKHV-Peterburg, SPb, 2010) (in Russian)
[17] E.D. Palik. *Handbook of Optical Constants of Solids* (Academic press, Orlando, 1985)
[18] A.B. Sotsky, S.S. Mikheev, M.M. Nazarov. Dokl. NAN Belarusi**63** (6), 672 (2019) (in Russian) DOI: 10.29235/1561-8323-2019-63-6-672-679
[19] A.B. Sotsky, M.M. Nazarov, S.S. Mikheev, L.I. Sotskaya. ZhTF, **91**(2), 315 (2020). (in Russian). DOI: 10.21883/JTF.2021.02.50368.199-20

[20] A.B. Sotsky, L.M. Shteyngart, S.O. Parashkov, L.I. Sotskaya. Izvestiya RAN. Ser. Phys., **80** (4), 465 (2016). DOI: 10.7868/S036767651604030X
[21] A. Piegari, E. Masetti. Thin Solid Films, **124**, 249 (1985). DOI: 10.1016/0040-6090(85)90273-1
[22] D. Bing, Y. Wang, J. Bai, R. Du, G. Wu, L. Liu. Opt. Commun., **406**, 128 (2018). DOI: 10.1016/j.optcom.2017.06.012
[23] Y. Ghim, H. Rhee. Opt. Lett., **44**, 5418 (2019). DOI: 10.1364/OL.44.005418
[24] N.I. Staskov, L.I. Sotskaya. J. Appl. Spectr., **84**, 764 (2017). DOI: 10.1007/s10812-017-0542-z

Translated by V.Prokhorov